PAPER • OPEN ACCESS

Defect processes in $Be_{12}X$ (X = Ti, Mo, V, W)

To cite this article: M.L. Jackson *et al* 2017 *Nucl. Fusion* **57** 086049

OPEN ACCESS
IOP Publishing | International Atomic Energy Agency
Nuclear Fusion
Nucl. Fusion **57** (2017) 086049 (10pp)
https://doi.org/10.1088/1741-4326/aa7b41

Defect processes in $Be_{12}X$ (X = Ti, Mo, V, W)

M.L. Jackson[1,2,4], P.A. Burr[3] and R.W. Grimes[1]

[1] Department of Materials, Centre for Nuclear Engineering, Imperial College London, SW7 2AZ, United Kingdom
[2] Culham Centre for Fusion Energy, Culham Science Centre, Abingdon, Oxfordshire, OX14 3DB, United Kingdom
[3] School of Electrical Engineering, University of New South Wales, Kingsford, NSW, 2052, Australia

E-mail: mj1809@ic.ac.uk

Received 23 January 2017, revised 3 June 2017
Accepted for publication 23 June 2017
Published 21 July 2017

Abstract

The stability of intrinsic point defects in $Be_{12}X$ intermetallics (where X = Ti, V, Mo or W) are predicted using density functional theory simulations and discussed with respect to fusion energy applications. Schottky disorder is found to be the lowest energy complete disorder process, closely matched by Be Frenkel disorder in the cases of $Be_{12}V$ and $Be_{12}Ti$. Antitisite and X Frenkel disorder are of significantly higher energy. Small clusters of point defects including Be divacancies, Be di-interstitials and accommodation of the X species on two Be sites were considered. Some di-interstitial, divacancy and X_{2Be} combinations exhibit negative binding enthalpy (i.e. clustering is favourable), although this is orientationally dependent. None of the $Be_{12}X$ intermetallics are predicted to exhibit significant non-stoichiometry, ruling out non-stoichiometry as a mechanism for accommodating Be depletion due to neutron transmutation.

Keywords: density functional theory, beryllide, beryllium

(Some figures may appear in colour only in the online journal)

Introduction

The use of beryllium (Be) in structural applications has been mostly limited to that of an alloying element, owing to the extreme toxicity of Be dust produced in machining. It is, nonetheless, employed due to its low atomic mass and unique neutronic properties; most notably as a window for x-rays and a neutron reflector and moderator in fission reactors [1].

Recently, Be has been used as a first wall material in experimental nuclear fusion reactors [2, 3], since it causes relatively small radiative losses in the event it contaminates the plasma during a transient event. In future reactors, Be is proposed as a neutron multiplying material for tritium (^{3}T) breeding [4–6], since ^{9}Be exhibits a low threshold for the (n, $2n$) reaction when bombarded with fast neutrons. In these applications, Be will be subject to temperatures of 600 °C [5, 7] and a high flux of neutrons resulting in the generation of ^{3}T and helium (He) through transmutation reactions. Several studies have indicated that this will cause an unacceptable degradation of its mechanical and thermal properties [8–10], along with retention of a high ^{3}T inventory, producing a radiological hazard [11, 12].

Be-rich intermetallics have been proposed as an alternative to elemental Be for nuclear applications, since they maintain similar neutronic properties to pure Be but perhaps offer a significant advantage in terms of ^{3}T retention and radiation tolerance [13, 14]. In particular, the $Be_{12}X$ series, where X is a transition metal, have proved promising, with studies showing that $Be_{12}Ti$ and $Be_{12}V$ have adequate neutronic properties for use as a multiplier [15]. In comparison to Be, however, the irradiation response of Be intermetallics has not yet been adequately characterised, although several studies have investigated the response of $Be_{12}Ti$, showing it to compare favourably to pure Be in terms of embrittlement, swelling and tritium retention [14].

Further work must be carried out to identify the fundamental processes occurring during radiation damage in Be

[4] Author to whom any correspondence should be addressed.

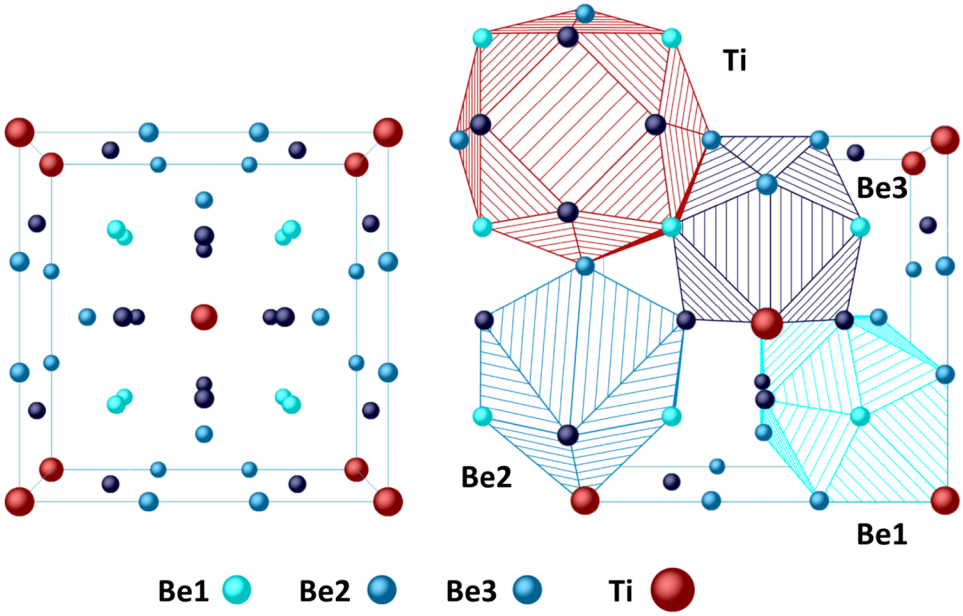

Figure 1. Left: position of stable Be and X interstitial sites within a unit cell of the I_4/mmm crystal structure of $Be_{12}X$, as viewed in the *c* direction. Right: coordination environment of symmetrically distinct lattice positions within the I_4/mmm crystal structure.

intermetallics. In particular, a greater understanding is required of how the point defects generated in damage cascades interact and lead to macroscopic changes in the microstructure. Recent work by Allouche *et al* [16] on the isomorphic $Be_{12}W$ structure used density functional theory to simulate the interactions of vacancies and hydrogen, finding that the intermetallic exhibits a significantly greater Be vacancy formation enthalpy in comparison to pure Be.

The study reported here contributes to our understanding of the fundamental processes occurring during radiation damage of Be intermetallics by predicting the formation and migration of intrinsic defects. It builds upon previous work focused on impurity behaviour in pure Be [17, 18].

After a brief description of the computational methodology, we review the crystal structure of the $Be_{12}X$ series, identifying all stable interstitial sites for intrinsic defects. The formation energies of all intrinsic point defects are evaluated, identifying the mechanisms relevant to stoichiometric, nonstoichiometric and radiation damage conditions.

Computational methodology

Density functional theory (DFT) simulations were mostly carried out using the Perdew, Burke and Ernzerhof (PBE) scheme of the generalised gradient approximation for the exchange-correlation functional [19]. Ultra-soft pseudo potentials with a consistent cut-off of 480 eV (converged to 10^{-3} eV atom^{-1}) were used throughout. All simulations were performed using the CASTEP code [20].

Defect calculations were performed in supercells constructed from $2 \times 2 \times 2$ full $Be_{12}X$ unit cells containing 208 atoms. A high density of *k*-points, with spacing of approximately 0.3 nm^{-1} was used for the integration of the Brillion Zone, following the Monkhost-Packing scheme [21]. This corresponds to *k*-point grids of $2 \times 2 \times 4$ for defect calculations.

As these materials are metallic, density mixing and Methfessel-Paxton [22] cold smearing of bands were employed with a width of 0.1 eV. Calculations were not spin-polarised, and during defect and elastic calculations no symmetry constraints were applied. All parameters, including the *k*-point spacing were converged to at least 10^{-3} eV atom^{-1}.

For atomic relaxation in defective cells, the energy convergence criterion for self-consistent calculations was set to 10^{-7} eV and that for the forces on atoms to less than 0.01 eV Å^{-1}. The cell was relaxed the stress component less than 0.05 GPa.

Crystallography

It has been established that the crystal structure of this family of materials exhibits tetragonal symmetry and spacegroup I_4/mmm [23]. Several studies also report $Be_{12}Ti$ as being hexagonal with spacegroup P_6/mmm [24, 25]. In fact, Gillam *et al* [23]. suggested that the large disordered hexagonal cell (with dimensions a = 29.44 and c = 7.33 Å) originally proposed by Raeuchle [25] is a derivative of the smaller tetragonal structure. This was confirmed in our recent work [26].

Within the I_4/mmm structure, the transition metal occupies the *2a* lattice site (0,0,0) with 20 fold coordination by Be (see figure 1). Be occupies three symmetrically distinct sites within the structure, here named *Be1*, *Be2* and *Be3*. The *Be1* site (¼,¼,¼) has *8f* symmetry, coordinated by 10 Be sites and two transition metal sites. The *Be2* site (*x*,0,0) has *8i* symmetry and is coordinated by 9 Be sites and one transition metal. Finally, the *Be3* site (*x*,½,0) has *8j* symmetry and is coordinated with 10 Be sites and two transition metal sites. Thus, the *Be2* and *Be3* sites exhibit special positions, so that different compounds with the same crystal structures have different position values.

Table 1. Lattice parameters, volumes and special positions calculated for the $Be_{12}X$ system, where X = V, Ti, Mo and W. x (Be_2) and x (Be_3) denotes the fractional x coordinate of these sites, which are special positions. Results calculated using the LDA functional are presented for comparison.

Lattice properties	$Be_{12}V$			$Be_{12}Ti$			$Be_{12}Mo$			$Be_{12}W$		
	Exp.	PBE	LDA	Exp.	PBE	LDA	Exp.	PBE	LDA	Exp.	PBE	LDA
a (Å)	7.266[a] 7.278[b]	7.240	7.127	7.35[c]	7.361	7.250	7.251[d] 7.271[b]	7.239	7.135	7.34 0 7.362[b]	7.227	7.126
c (Å)	4.194[a] 4.212[b]	4.169	4.104	4.19[c]	4.163	4.098	4.232[d] 4.234[b]	4.221	4.164	4.216[e] 4.232[b]	4.223	4.167
V (Å^3)	221.4[a] 223.1[b]	218.5	208.5	226.4[c]	225.6	215.4	222.5[d] 223.8[b]	221.2	211.9	227.1[e] 229.4[b]	220.6	211.6
x (Be_2)	0.361[a]	0.349	0.348	—	0.350	0.351	0.351[b]	0.350	0.350	0.351[f]	0.351	0.351
x (Be_3)	0.277[a]	0.288	0.289	—	0.281	0.283	0.281[b]	0.289	0.289	0.290[f]	0.290	0.289

[a] Reference [27].
[b] Reference [28].
[c] Reference [29].
[d] Reference [30].
[e] Reference [31].
[f] Reference [31].

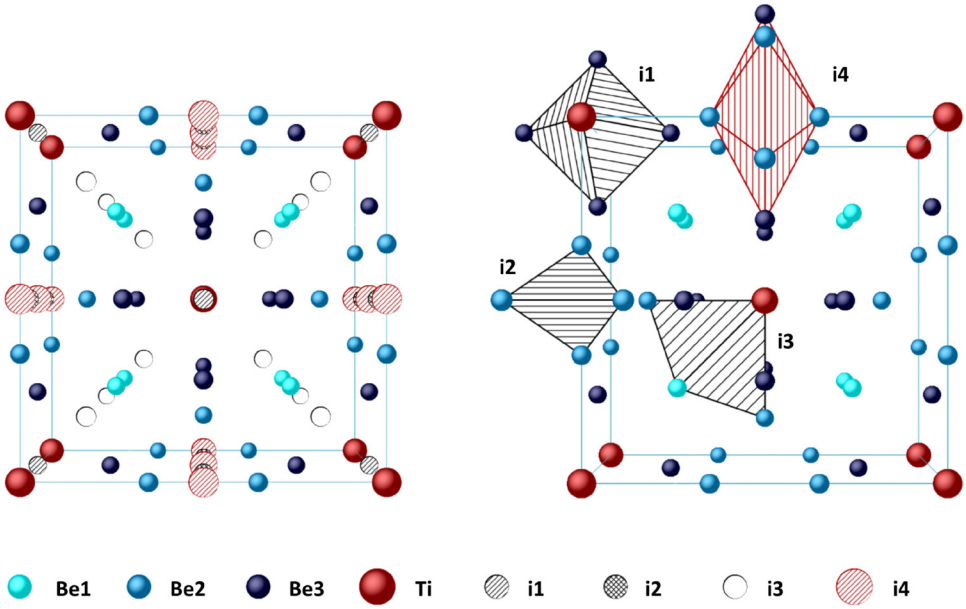

Figure 2. Left: interstitial positions within a unit cell of the $Be_{12}X$ structure as viewed along the c direction. Right: coordination environment of the four interstitial sites.

To part validate the choice of the model, and in particular the choice of the exchange-correlation functional, the calculations of perfect crystals structures were performed using the local density approximation (LDA) and PBE functional, the results of which are compared with experimental data in table 1. It is clear that results generated using PBE are in closer agreement with experiment than LDA. (Further comparison between PBE and LDA results are discussed later: in figure 3 for phase stability and for the formation energies of vacancy and anti-site defects in $Be_{12}Ti$ in the appendix—table A2.) The simulated lattice volumes are ~1% below their experimental volumes, typical for DFT predictions on metallic and intermetallic systems when using the PBE exchange correlation terms [19], and significantly closer to the experimental value than those predicted using the LDA functional.

While the perfect structure of this family of materials has been well characterised, interstitial sites within the $I4/mmm$ structure are identified here for the first time. This is achieved using the brute force approach described by Murphy [32], by seeding a $Be_{12}Ti$ unit cell with a dense grid of Be and Ti interstitials with 0.03 nm spacing and performing a single point calculation to find the energy of these (unrelaxed) sites. The 20 lowest energy and symmetrically distinct defects were reproduced in a $2 \times 2 \times 2$ supercells and geometry optimised to find the final position of the interstitial site. Four interstitial sites were identified as present within the $I4/mmm$ structure in figure 2. Three interstitial sites can accommodate both Be and Ti, a *2b* site labelled *i1*, a *4b* site labelled *i2*, and an *8h* site labelled *i3*. The Wyckoff notation uniquely describes their location. A further site was found to be stable for the X species at (0,½,½) (*4c* symmetry) and is labelled *i4*. Be interstitials placed on this

Table 2. Formation enthalpies, E_f, of unbound Be vacancies and interstitials. $Be_{12}W$ is compared to previous DFT data. In bold, the most favourable defect of each type.

	E_f/defect (eV)						
Defect	$Be_{12}V$	$Be_{12}Ti$	$Be_{12}Mo$	$Be_{12}W$	$Be_{12}W$[a]	Defect	Be[b]
Be vacancies						Be vacancies	
V_{Be1}	1.59	1.60	1.59	1.38	1.38	V_{Be}	1.09
V_{Be2}	**1.48**	**1.43**	**1.34**	**1.20**	**1.14**	Be interstitials	
V_{Be3}	1.64	1.53	1.66	1.47	1.48	Be_i (Oc)	5.06
Be interstitials						Be_i (Te)	5.14
Be_{i1}	2.95	3.19	3.54	3.81	—	Be_i (NBt)	4.77
Be_{i2}	**2.03**	**1.86**	**2.37**	**2.50**	—	Be_i (Hx)	5.67
Be_{i3}	3.54	3.69	3.92	4.14	—	Be_i (Tr)	4.01

[a] Allouche *et al* (DFT data) [16].
[b] Middleburgh and Grimes (DFT data) [17].

Table 3. Formation enthalpies of unbound transition metal vacancies and interstitials, presented in order of increasing transition metal radii. In bold, the lowest energy interstitial.

	E_f/defect (eV)				
Defect	$Be_{12}V$	$Be_{12}Ti$	$Be_{12}Mo$	$Be_{12}W$	$Be_{12}W$[a]
X vacancies					
V_X	3.37	4.10	3.61	3.16	3.25
X interstitials					
X_{i1}	4.81	5.37	7.26	8.11	—
X_{i2}	4.79	5.10	5.60	6.48	—
X_{i3}	5.59	7.47	8.80	10.11	—
$\mathbf{X_{i4}}$	**4.69**	**4.19**	**4.84**	**5.95**	—

[a] Allouche *et al* [16] (DFT data).

Table 4. Defect formation enthalpies for antisite defects in the $Be_{12}X$ series, presented in order of increasing atomic radii of the transition metal species. In bold, the lowest energy antisite.

	E_f/defect (eV)			
Defect	$Be_{12}V$	$Be_{12}Ti$	$Be_{12}Mo$	$Be_{12}W$
Anti-site				
Be_X	2.83	3.55	3.09	2.76
X_{Be1}	3.10	3.26	4.13	4.43
$\mathbf{X_{Be2}}$	**0.99**	**0.95**	**1.56**	**3.81**
X_{Be3}	1.79	2.50	3.40	3.81

Table 5. Binding energies (where negative means bound and positive means unstable) of Be and X vacancies with respect to V_{Be2} and V_x. In bold, the most favourable divacancy cluster of each type.

	E_B (eV)			
Divcacancy	$Be_{12}V$	$Be_{12}Ti$	$Be_{12}Mo$	$Be_{12}W$
$V_{Be3}V_{Be3}$ (in plane)	0.37	0.41	0.74	0.92
$V_{Be3}V_{Be3}$ (out of plane)	0.37	0.44	0.35	0.74
$V_{Be2}V_{Be3}$ (in plane)	0.04	0.30	0.70	0.46
$V_{Be2}V_{Be3}$ (out of plane)	−0.08	0.04	0.12	0.19
$V_{Be2}V_{Be2}$ (in plane)	−0.01	0.22	0.03	0.11
$V_{Be2}V_{Be2}$ (in plane)	−0.08	0.35	0.12	0.22
$\mathbf{V_{Be2}V_{Be2}}$ **(out of plane)**	**−0.21**	**−0.04**	**−0.09**	**−0.02**
$V_{Be2}V_{Be1}$	−0.04	0.26	0.25	0.33
$V_{Be1}V_{Be1}$	0.23	0.38	0.56	0.65
$V_{Be1}V_{Be3}$	0.16	0.63	0.46	0.52
V_XV_X	0.75	0.50	0.58	0.72
V_XV_{Be3}	−0.04	−0.04	0.17	0.22
$\mathbf{V_xV_{Be2}}$	**−0.54**	**−0.41**	**−0.29**	**−0.19**
V_XV_{Be1}	0.04	−0.02	0.37	0.42

site move to a neighbouring *Be3* site, displacing the Be atom to the *i1* site when geometry optimised. In all cases, these present as typical interstitials in a complex structure, remaining on high symmetry sites and perturbing the surrounding lattice in a roughly symmetrical manner rather than forming a dumbbell as is common in simple metallic structures [33, 34].

Point defects

The formation enthalpies (E_f) of a Be vacancy and interstitial, denoted in Kröger–Vink notation [35] V_{Be} and Be_i, are presented relative to their elemental reference states in table 2, following for example:

$$Be_{Be} \rightarrow V_{Be} + Be_{(s)}$$

For these materials, the V_{Be2} site systematically exhibits the lowest E_f. V_{Be1} has the next highest E_f, except for $Be_{12}Ti$ where the order of the *Be2* and *Be3* sites is reversed. For all cases there is only a small relative difference in E_f between all three sites, reaching a maximum of 0.32 eV for V_{Be2} and V_{Be3} in $Be_{12}Mo$. For Be_i the *i2* site systematically exhibits the lowest E_f, with the *i1* and *i3* sites significantly higher. All Be_i species have considerably higher E_f than V_{Be} species.

The formation energies of V_X and X_i are presented in table 3. Both V_X and X_i have significantly higher E_f than V_{Be} and Be_i. For all materials V_X exhibit lower E_f than the lowest enthalpy interstitial site, X_{i4}.

Another important defect process resulting from radiation damage is antisite disorder, the E_f of which are presented in table 4. In all materials the accommodation of Be on a X site has a large energy penalty, likely due to the size mismatch between Be and the X species. The lowest E_f defect is X_{Be2}, likely as this site is only coordinated with one X site rather

Table 6. Binding enthalpies (where negative means bound and positive means unstable) of Be_i Be_i with respect to two Be_{i2}. In Bold, the most favourable di-interstitial cluster.

	Binding enthalpy (eV)			
Interstitial sites	$Be_{12}V$	$Be_{12}Ti$	$Be_{12}Mo$	$Be_{12}W$
$Be_{i2}Be_{i2}$	0.38	0.71	0.37	0.42
$Be_{i3}Be_{i1}$ (in plane)	1.90	2.41	2.18	2.32
$Be_{i3}Be_{i1}$ (out plane)	1.98	2.50	2.10	2.22
$Be_{i3}Be_{i2}$	0.34	0.17	0.69	0.71
$Be_{i3}Be_{i3}$	1.69	2.50	1.82	1.86
$Be_{i3}Be_{i4}$ (in plane)	1.74	2.17	2.01	2.16
$Be_{i3}Be_{i4}$ (out plane)	1.96	2.42	0.69	0.71
$Be_{i4}Be_{i2}$	0.43	0.38	0.32	0.38
$Be_{i4}Be_{i4}$	**−0.10**	**−0.10**	**0.08**	**0.09**

Table 7. Binding enthalpy (where negative means bound and positive means unstable) of X_{2Be} with respect to X_{Be2} and V_{Be2}. In bold, the most favourable cluster for each material.

	Binding enthalpy (eV)			
Anti-site vacancy pair	$Be_{12}V$	$Be_{12}Ti$	$Be_{12}Mo$	$Be_{12}W$
$X_{Be3–Be3}$ (in plane)	0.33	1.35	0.63	−1.77
$X_{Be3–Be3}$ (out of plane)	−0.42	0.17	−0.16	−1.28
$X_{Be2–Be3}$ (in plane)	−0.51	−0.09	−0.45	−1.48
$X_{Be2–Be3}$ (out of plane)	**−2.46**	−0.91	**−2.88**	−2.04
$X_{Be2–Be2}$ (in plane)	−0.40	4.26	−0.02	−1.77
$X_{Be2–Be2}$ (in plane)	3.44	0.00	−0.32	−1.67
$X_{Be2–Be2}$ (out of plane)	−0.40	**−3.02**	0.17	**−4.55**
$X_{Be2–Be1}$	−0.06	−0.38	−0.16	−2.22
$X_{Be1–Be3}$	0.75	−0.46	0.54	−1.93
$X_{Be1–Be2}$	0.75	0.00	0.03	−1.01

than two as for the Be1 and Be3 sites. In the case of $Be_{12}W$ the energy penalty for accommodating X on a Be site is noticeably larger than for other materials.

Defect clustering

Since larger defects such as voids might form through coalescence of smaller clusters, how defects interact, particularly whether there is a driving force for association, is a key indicator of how the microstructure of a material will evolve during irradiation. As an initial step towards cluster formation, the binding enthalpies E_B of nearest neighbour vacancies and interstitials were calculated with respect to the lowest enthalpy isolated defect of each type, that is, two V_{Be2} or two Be_{i2} (see table 5). Also, the cluster X_{2Be} was considered, formed from X_{Be} and V_{Be} (which provides more volume for the larger X atom than a single vacancy). In all cases the propensity to form a cluster is indicated as a negative binding energy, for example,

Table 8. Normalised defect process formation energies, E_f, for Frenkel, Schottky and (simple) antisite disorder.

	E_f/defect (eV)			
Defect	$Be_{12}V$	$Be_{12}Ti$	$Be_{12}Mo$	$Be_{12}W$
Be Frenkel	1.76–2.59	1.64–2.65	1.85–2.79	1.85–2.81
X Frenkel	4.03–4.48	4.15–5.78	4.22–6.20	4.55–6.63
Schottky	1.63–1.77	1.63–1.79	1.51–1.81	1.35–1.60
Antisite	1.91–2.96	2.25–3.41	2.33–3.61	3.29–3.60

Table 9. Solution energy to closest compositional reference state that results in the formation of a single defect and hence a change in stoichiomtry. Governing equations can be found in the appendix.

	E_f/defect (eV)			
Defect	$Be_{12}Ti$	$Be_{12}V$	$Be_{12}Mo$	$Be_{12}W$
V_{Be}	1.52	1.53	1.36	1.26
V_X	3.34	3.23	1.46	1.41
Be_i	2.49	2.34	2.23	2.37
X_i	6.04	5.39	5.64	6.76
Be_X	2.79	2.66	0.81	0.88
X_{Be}	2.98	1.78	2.39	4.67
X_{2Be}	1.48	0.84	0.88	1.38
$V_{Be}V_{Be}$	2.82	2.97	2.64	2.49
V_XV_{Be}	4.45	4.19	2.54	2.47
V_XV_X	7.18	7.17	3.50	3.54
Be_iBei	4.89	4.59	4.54	4.82

$$V_{Be2} + V_{Be2} \rightarrow V_{Be2}V_{Be2} \ \text{(Out of plane)}$$

which is the lowest energy orientation cluster incorporating two lowest energy isolated vacancies (where out of plane indicates the two vacancies are orientated out of the basal plane). Alternately,

$$V_{Be2} + V_{Be2} + Be_{Be1} + Be_{Be3} \rightarrow V_{Be1}V_{Be3} + 2Be_{Be2}$$

will yield the binding energy to form the $V_{Be1}V_{Be3}$ cluster from two (lowest energy) isolated V_{Be2} defects (which is positive and thus the cluster is not stable).

Table 5 *shows that f*or all materials the strongest cluster association by far is between V_{Be2} and V_X, while two V_X defects are strongly repelled in all materials. That some orientations of the $V_{Be}V_{Be}$ and $V_{Be}V_X$ divacancy are favourable suggests such clusters may act as nucleation sites for void formation, however, given that this cluster energy is strongly orientation dependent, further simulations of larger clusters are required to validate such a hypothesis.

Values of E_B for two Be_i on nearest neighbour sites are presented in table 6. Be_iBe_i clusters include those on the *i4* site, despite this site not being stable for individual Be_i defects. For most materials and interstitial combinations, $E_B(Be_iBe_i)$ is repulsive, thus there is usually no driving force to form such clusters. One exception to this is $E_B(Be_{i4}Be_{i4})$ which is slightly

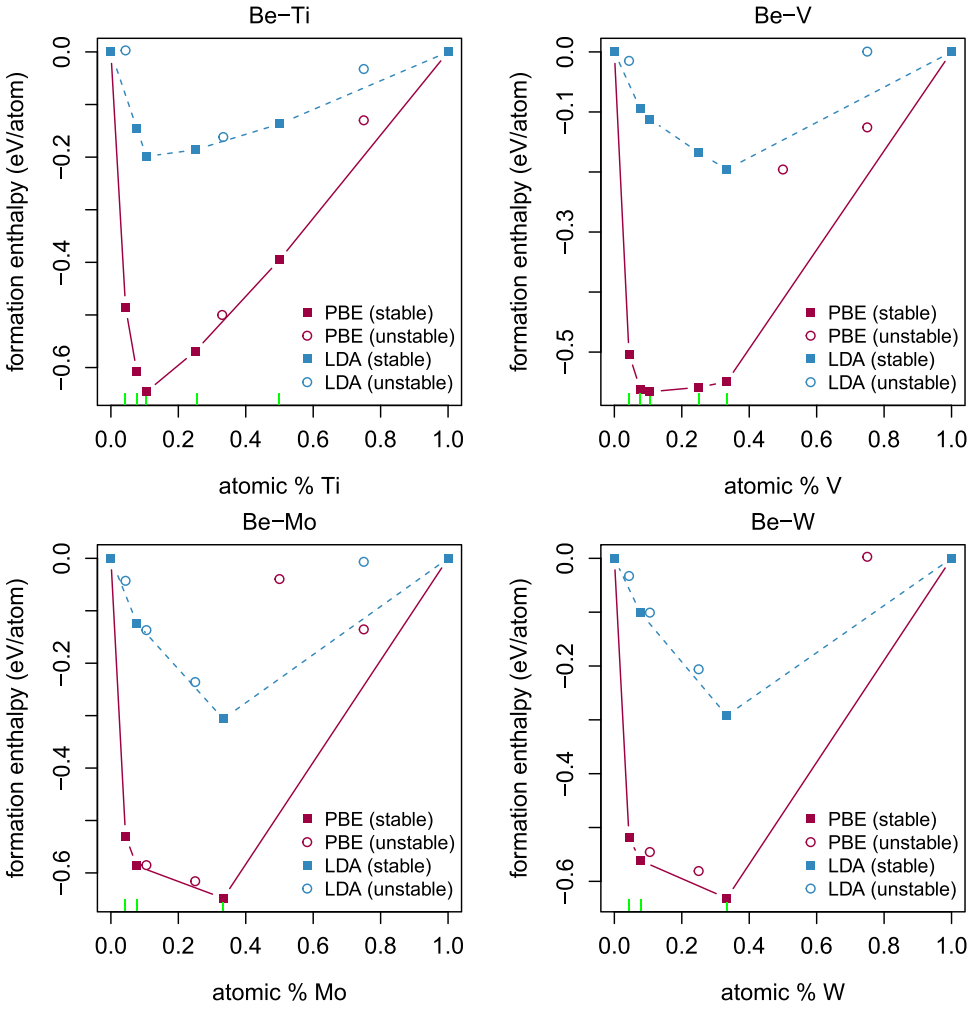

Figure 3. Convex hull analysis of the Be–Ti, Be–V, Be–Mo and Be–W systems as calculated using the LDA and PBE functionals. Phases exhibiting positive formation energies are not included.

negative in both $Be_{12}Ti$ and $Be_{12}V$ and only moderately repulsive in $Be_{12}Mo$ and $Be_{12}W$. Thus, we predict no driving force for the formation of larger interstitial defect clusters, through a model where isolated interstitial defects associate initially into pairs, other than via two interstitials reorienting onto *i4* sites.

The binding energies for V_{Be} and X_{Be} to form X_{2Be} are presented in table 7. E_B ranges from strongly negative (−4.55 eV) to strongly positive (4.26 eV). The lowest energy sites are split between *Be2–Be3* for $Be_{12}V$ and $Be_{12}Mo$, and *Be2–Be2* for $Be_{12}Ti$ and $Be_{12}W$. The latter case might have been anticipated, as this position corresponds roughly to the arrangement of atoms in the $Be_{17}Ti_2$ Pc/mmm phase, which is closely related to the $Be_{12}Ti$ I_4/mmm phase [23].

Defect disorder processes

Defects can be generated in a material through several different processes (disorder reactions) that can occur thermally, or be driven by radiation damage cascades. Table 8 shows the energies associated with Frenkel, Schottky and Antisite processes (normalised by the number of defects for each process).

The range of E_f values for vacancy, interstitial and antisite defects leads to a range of values for each disorder process, which can vary by as much as 2 eV or as little as 0.2 eV. While the minimum value could be the most significant in equilibrium processes, radiation damage is not an equilibrium process and thus higher enthalpy configurations may also be important.

For all of these materials, Schottky disorder is the lowest enthalpy disorder process, while Be Frenkel disorder exhibits a similar albeit slightly higher energy. Indeed for $Be_{12}Ti$, Schottky and Frenkel disorder energies are essentially identical. Conversely, X Frenkel disorder is a much higher energy process in all materials. Thus, we predict a strong thermodynamic driving force for the removal of X_i species from a damaged lattice. In the case of $Be_{12}V$, antisite disorder will also be significant, being within 0.3 eV/defect of the Schottky process.

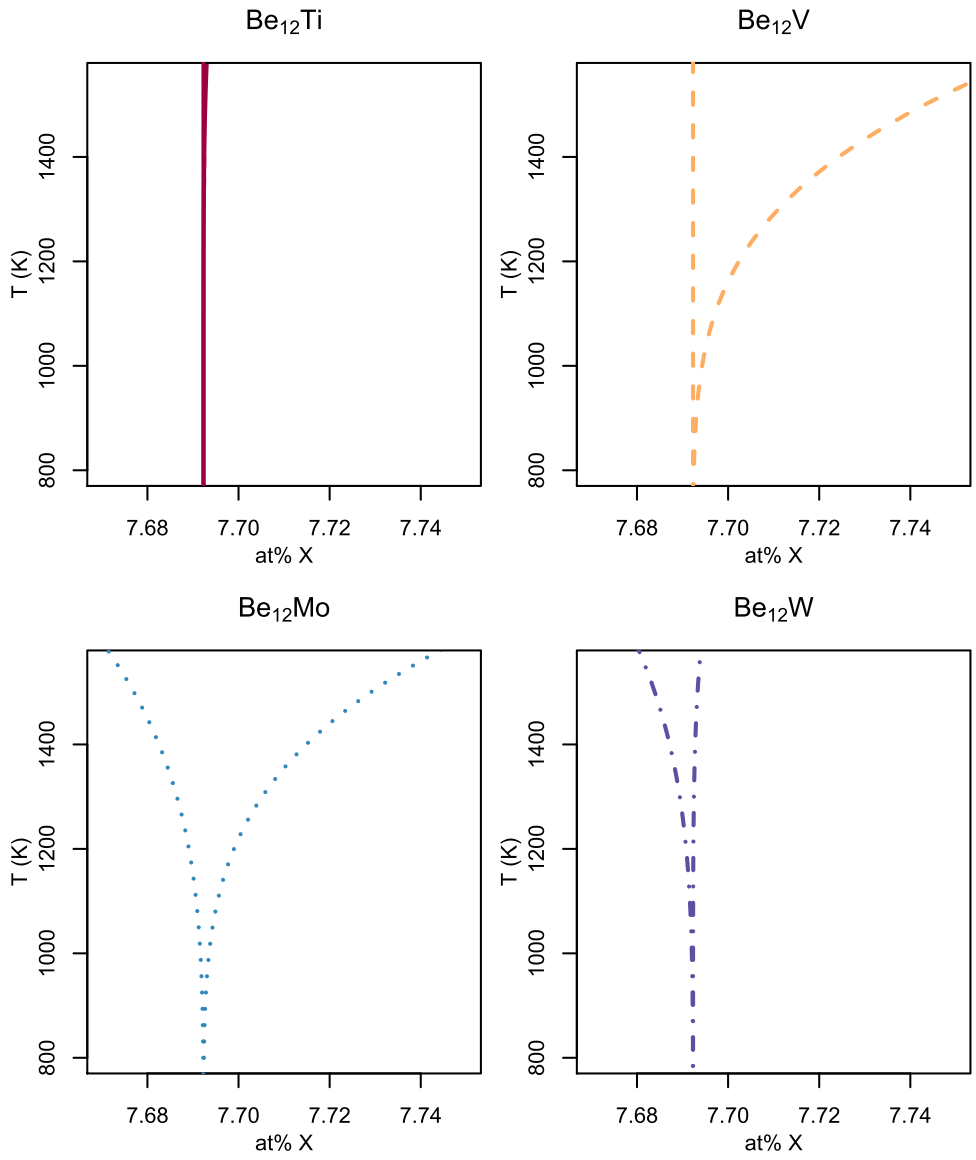

Figure 4. Predicted phase field lines based on total defect concentrations predicted through the Arrhenius approximation for materials with an excess of Be and the X species.

Nonstochiometry

In neutron multiplier materials ^{9}Be atoms are depleted to generate additional neutrons. Thus, it is important to understand the stability of Be-X phases at different Be contents. First we investigate a wide range of Be-X compositions through convex hull analyses, then we focused on small deviation of stoichiometry from the $Be_{12}X$ composition. Figure 3 shows the convex hulls obtained for all four Be-X series. For completeness, these calculations were repeated with LDA exchange-correlation functional.

Within this analysis, all phases that lie on the line of lowest-energy phases are predicted to be stable, while those that lie above the convex hull are predicted to be unstable (notwithstanding temperature effects). Formation energies obtained with the PBE functional are significantly lower than those obtained with LDA, consistent with the fact that LDA calculations are known to over-delocalise electrons, which may lead to an apparent increase in stability of the parent metals. Nevertheless, except for $Be_{22}X$, the two methods are qualitatively in agreement with one-another. $Be_{22}X$ is consistently predicted unstable with LDA and stable with PBE, while experimentally it is known to be stable (at room temperature) for W and Mo but unstable for Ti and V [36–39].

The PBE convex hulls for Be-Mo and Be-W are in perfect agreement with experimental phase diagrams [37, 38], reporting only three stable compositions: $Be_{22}X$, $Be_{12}X$ and Be_2X, with all other candidate phases lying well above the convex hull. A single study also reports the formation of $BeMo_3$ [40], but this has not been confirmed by subsequent experiments. Our calculations predict this phase to be unstable.

The Be-Ti and Be-V phase diagrams are more complex: the simulation results are in agreement with the experimental literature regarding the stability of $Be_{12}Ti$, $Be_{12}V$, $Be_{17}Ti_2$, $Be_{17}V_2$, Be_2Ti and Be_2V; but in contrast to the experimental observation, $Be_{22}Ti$, $Be_{22}V$ and Be_3V are also predicted to be stable (with the PBE functional), while Be_3Ti is predicted to be unstable by a small margin [36]. It is important to note that the formation energies of these phases lie within meVs of the boundary of stability. Thus, these discrepancies are likely attributed to temperature effects (both enthalpy and entropy), as was shown to be the case for the closely-related Be–Fe and Be–Fe–Al systems [18].

To assess the possible deviation from stoichiometry that $Be_{12}X$ phases may accommodate, one needs to consider the formation of defects that lead to non-stoichiometry against the formation of a phase with neighbouring composition. This is quantified by the energy to dissolve a formula unit of the nearest 0 K reference state into $Be_{12}X$, creating defects in the $Be_{12}X$ lattice. For instance in the case of $Be_{12}Ti$, where $Be_{17}Ti_2$ phase incorporation results in V_{Be} formation:

$$Be_{17}Ti_2 + 7Be_{Be} \leftrightarrow 7\ V_{Be} + 2Be_{12}T$$

where Be_{Be} are Be atoms on Be sites in the host $Be_{12}Ti$ lattice. A full list of these equations and reference states (which are chosen using a convex hull analysis) is presented table A1 in the appendix. The minimum energy for the incorporation of reference states is shown in table 9. The number of defects formed can then be calculated at temperature using the Arrhenius approximation and total deviation from stoichiometry calculated, as presented in figure 4.

All compounds exhibit almost no deviation from stoichiometry (note that the full range of the ordinate axis corresponds to a compositional variation of 0.08 at%). This is especially true for $Be_{12}Ti$, while $Be_{12}V$ may accommodate limited Be sub-stoichiometry, $Be_{12}W$ may accommodate very minor levels of Be hyper-stochiometric, and $Be_{12}Mo$ may accommodate small deviation on both side of the stoichiometric composition. This difference in behaviour can be attributed to the relative energy of the three lowest energy defect reactions resulting in V_{Be} X_{Be} and X_{2Be} formation. In $Be_{12}Ti$ the lowest energy defect is Ti_{2Be} with energy 1.48 eV, considerably higher than for other materials thereby promoting little deviation from stoichiometry. In the case of $Be_{12}V$, V_{2Be} has a lowest energy, 0.84 eV, so that any non-stoichiometry will be accommodated by an excess of the transition metal. A similar profile occurs in $Be_{12}Mo$, where Mo_{2Be} has energy 0.88 eV, however Be_{Mo} has formation energy 0.81 eV which also allows for some non-stochiometry in the Be rich region. $Be_{12}W$ becomes hyperstochiometric as Be_W has energy 0.88 eV.

The extent of non-stochiometry predicted in these materials is such as they may be considered line compounds. Thus, upon depletion of Be due to the (*n*,2*n*) reaction, these materials are likely to form secondary phases with composition $Be_{17}V_2$, $Be_{17}Ti_2$, Be_2W and Be_2Mo, to accommodate excess X. From this point of view, $Be_{12}V$ and $Be_{12}Ti$ are likely to be the least affect by the formation of secondary phases, not because of their ability to accommodate deveiations from stoicbiometry, but because the secondary phases have structural similarities to the parent phase [23] and not too dissimilar composition. Following the same logic, $Be_{22}W$ and $Be_{22}Mo$ should be considered as possible candidates over $Be_{12}W$ and $Be_{12}Mo$.

Conclusions

Density functional theory simulations have been carried out to predict defect properties of $Be_{12}X$ materials. The PBE functional yielded better agreement with experiment compared to the LDA functional, both in terms of phase stability and lattice parameters (within 1% for PBE). Formation enthalpies of all possible vacancies, interstitials and anti-site point defects were calculated for all four materials. Four stable sites for intrinsic interstitials are identified for the first time in the I_4/mmm structure: the *i2* site (*4b*) is most stable for Be self-interstitials but for X_i species, the *i*4 (*4c*) site offers a similar or lower energy. In all cases, the Be sub-lattice accommodates defects more readily than the X sub-lattice. Formation energies of point defects were combined to predict the energies of intrinsic disorder processes. Of these, Schottky disorder was identified as the lowest energy process, while Be Frenkel disorder exhibited only slightly higher energy for the V and Ti containing materials.

Small clusters including $V_{Be}V_{Be}$, Be_iBe_i and X_{2Be} were investigated, with some combinations exhibiting favourable binding enthalpy, particularly for X_{2Be}, which in some cases has a notably lower enthalpy than that of simple antisite disorder. This is likely due to the large size discrepancy between Be and the X species.

$Be_{12}Mo$, $Be_{12}V$ and $Be_{12}W$ can only exhibit modest non-stoichiometry at elevated temperatures, while $Be_{12}Ti$ is essentially a true line compound due the relatively high energy required to form a defect relative to its nearest reference state. The ability to accommodate the removal of Be atoms (X excess) without severely affecting the compounds stability is a noteworthy property for neutron multiplier purposes, where Be atoms are continually consumed to maintain the necessary neutron flux. Consideration of which secondary phases might form is therefore important.

Acknowledgments

MLJ has received funding via CCFE from the Euratom research and training programme 2014–2018 under grant agreement No 633053 (EUROfusion Consortium)—the views and opinions expressed herein do not necessarily reflect those of the European Commission. Computing resources were provided by the Imperial College London High Performance Computing Service. Dr Dmitry Bachurin is acknowledged for his useful insight on the possible importance of X species accommodation on a Be divacancy. We would like to thank the reviewer for his suggestion to add the convex hulls analysis. RWG would like to acknowledge support from EPSRC grant reference EP/I003088/1.

Appendix

Table A1. Reference states and defect equations evaluated to calculate non-stochiometry.

Material	$Be_{12}W$ and $Be_{12}Mo$	$Be_{12}Ti$ and $Be_{12}V$
Reference states	$Be_{22}W/Be_2W$, $Be_{22}Mo/Be_2Mo$	$Be/Be_{17}Ti_2$, $Be/Be_{17}V_2$
V_{Be}	$Be_2X + 10Be_{Be} \leftrightarrow 10V_{Be} + Be_{12}X$	$Be_{17}X_2 + 7Be_{Be} \leftrightarrow 7V_{Be} + 2Be_{12}X$
V_X	$6Be_{22}X + 5X_X \leftrightarrow 5V_X + 11Be_{12}X$	$12Be + X_X \leftrightarrow V_X + Be_{12}X$
Be_i	$Be_{22}X \leftrightarrow 10Be_i + Be_{12}X$	$Be_{17}X_2 + 8Be \leftrightarrow 2Be_{12}X + Be_i$
X_i	$6Be_2X \leftrightarrow 5X_i + Be_{12}X$	$12Be_{17}X_2 \leftrightarrow 7X_i + 17Be_{12}X$
$2V_{Be}$	$Be_2X + 10Be_{Be} \leftrightarrow 5(2V_{Be}) + Be_{12}X$	$2Be_{17}X_2 + 14Be_{Be} \leftrightarrow 7(2V_{Be}) + 4Be_{12}X$
$2V_X$	$12Be_{22}X + 5X_X \leftrightarrow 5(2V_X) + 22Be_{12}X$	$24Be + 2X_X \leftrightarrow (2V_X) + 2Be_{12}Ti$
$V_{Be}V_X$	$11Be_{22}X + 10X_X + 10Be_{Be} \leftrightarrow 10V_{Be}V_X + 21Be_{12}X$	$11Be + Be_{Be} + Ti_{Ti} \leftrightarrow V_{Be}V_{Ti} + Be_{12}Ti$
$2Be_i$	$Be_{22}X \leftrightarrow 5(2Be_i) + Be_{12}X$	$2Be_{17}Ti_2 + 16Be \leftrightarrow 4Be_{12}Ti + (2Be_i)$
Be_X	$13Be_{22}X + 10X_X \leftrightarrow 10Be_X + 23Be_{12}X$	$13Be + Be_{Be} + Ti_{Ti} \leftrightarrow Be_{Ti} + Be_{12}Ti$
X_{Be}	$13Be_2X + 10Be_{Be} \leftrightarrow 10X_{Be} + 3Be_{12}X$	$2Be_{17}Ti_2 + Be_{Be} + Be \leftrightarrow Ti_{Be} + 3Be_{12}Ti$
X_{2Be}	$14Be_2X + 20Be_{Be} \leftrightarrow 10X_{2Be} + 4Be_{12}X$	$2Be_{17}Ti_2 + 2Be_{Be} \leftrightarrow Ti_{2Be} + 3Be_{12}Ti$

Table A2. Defect formation energies of vacancies and anti-sites in $Be_{12}Ti$ calculated with PBE and LDA, showing qualitative agreement between the two functionals.

	E_f^{PBE}(eV)	E_f^{LDA} (eV)
V_{Be1}	1.60	1.81
V_{Be2}	1.43	1.62
V_{Be3}	1.53	1.73
V_{Ti}	4.10	4.32
Be_{Ti}	3.55	3.56
Ti_{Be1}	3.26	3.52
Ti_{Be2}	0.92	1.08
Ti_{Be3}	2.50	2.62

References

[1] Tomberlin T.A. 2004 *Beryllium—a Unique Material in Nuclear Applications* (Idaho Falls, ID: Idaho National Laboratory)

[2] Smith M.F. and Mullendore A.W. 1984 An evaluation of beryllium for magnetic fusion components *J. Nucl. Mater.* **122** 855–7

[3] Deksnis E.B., Peacock A.T., Altmann H., Ibbot C. and Falter H.D. 1997 Beryllium plasma-facing components: JET experience *Fusion Eng. Des.* **37** 515–30

[4] Giancarli L.M. *et al* 2012 Overview of the ITER TBM program *Fusion Eng. Des.* **87** 395–402

[5] Tobita K., Utoh H., Liu C., Tanigawa H., Tsuru D., Enoeda M., Yoshida T. and Asakura N. 2010 Search for reality of solid breeder blanket for DEMO *Fusion Eng. Des.* **85** 1342–7

[6] Tsuchiya K. *et al* 2007 Development of advanced tritium breeders and neutron multipliers for DEMO solid breeder blankets *Nucl. Fusion* **47** 1300–6

[7] Zmitko M., Poitevin Y., Boccaccini L., Salavy J.-F., Knitter R., Möslang A., Magielsen A.J., Hegeman J.B.J. and Lässer R. 2011 Development and qualification of functional materials for the EU test blanket modules: strategy and R&D activities *J. Nucl. Mater.* **417** 678–83

[8] Gelles D.S. and Heinisch H.L. 1992 Neutron damage in beryllium *J. Nucl. Mater.* **191** 194–8

[9] Chakin V., Rolli R., Moeslang A., Vladimirov P., Kurinskiy P., van Til S., Magielsen A.J. and Zmitko M. 2013 Characterization of constrained beryllium pebble beds after neutron irradiation at HFR at high temperatures up to helium production of 3000 appm *Fusion Eng. Des.* **88** 2309–13

[10] Chakin V.P., Posevin A.O. and Latypov R.N. 2006 Radiation damage in beryllium at 70–440 °C and neutron fluence (0.3–18)· $\times 10^{22}$ cm^{-2} (En > 0.1 MeV) *At. Energy* **101** 743–9

[11] Billone M.C., Lin C.C., Baldwin D.L. and Argonne National Lab 1990 *Tritium and Helium Behavior in Irradiated Beryllium* (Richland, WA: Pacific Northwest Lab)

[12] Rabaglino E., Hiernaut J.P., Ronchi C. and Scaffidi-Argentina F. 2002 Helium and tritium kinetics in irradiated beryllium pebbles *J. Nucl. Mater.* **307–11** 1424–9

[13] Uchida M., Ishitsuka E. and Kawamura H. 2002 Tritium release properties of neutron-irradiated $Be_{12}Ti$ *J. Nucl. Mater.* **307–11** 653–6

[14] Neubauer O. *et al* 2013 Characteristics of microstructure, swelling and mechanical behaviour of titanium beryllide samples after high-dose neutron irradiation at 740 and 873 K *Fusion Eng. Des.* **88** 2198–201

[15] Yamada H., Nagao Y., Kawamura H., Nakao M., Uchida M. and Ito H. 2003 Preliminary neutronic estimation for demo blanket with beryllide *Fusion Eng. Des.* **69** 269–73

[16] Allouche A., Fernandez N. and Ferro Y. 2014 Hydrogen retention and diffusion in tungsten beryllide *J. Phys.: Condens. Matter* **26** 315012

[17] Middleburgh S.C. and Grimes R.W. 2011 Defects and transport processes in beryllium *Acta Mater.* **59** 7095–103

[18] Burr P.A., Middleburgh S.C. and Grimes R.W. 2015 Crystal structure, thermodynamics, magnetics and disorder properties of Be–Fe–Al intermetallics *J. Alloys Compd.* **639** 111–22

[19] Perdew J.P., Burke K. and Ernzerhof M. 1996 Generalized gradient approximation made simple *Phys. Rev. Lett.* **77** 3865–8

[20] Segall M.D., Lindan P.J.D., Probert M.J., Pickard C.J., Hasnip P.J., Clark S.J. and Payne M.C. 2002 First-principles simulation: ideas, illustrations and the CASTEP code *J. Phys.: Condens. Matter* **14** 2717–44

[21] Monkhorst H.J. and Pack J.D. 1976 Special points for Brillouin-zone integrations *Phys. Rev.* B **13** 5188–92

[22] Methfessel M. and Paxton A. 1989 High-precision sampling for Brillouin-zone integration in metals *Phys. Rev.* B **40** 3616–21

[23] Gillam E., Rooksby H.P. and Brownlee L.D. 1964 Structural relationships in beryllium–titanium alloys *Acta Crystallogr.* **17** 762–3

[24] Liu X.K., Zhou W., Liu X. and Peng S.M. 2015 First-principles investigation of the structural and elastic properties of $Be_{12}Ti$ under high pressure *RSC Adv.* **5** 59648–54
[25] Raeuchle R.F. and Rundle R.E. 1952 The structure of $TiBe_{12}$ *Acta Crystallogr.* **5** 85–93
[26] Jackson M.L., Burr P.A. and Grimes R.W. 2016 Resolving the structure of $TiBe_{12}$ *Acta Crystallogr.* B **72** 277–80
[27] Kripyakevich P.I. and Gladyshevskii E.I. 1955 KRISTALLICHESKAYA STRUKTURA SOEDINENII CRBE12, VBE12 I NBBE12 *DOKLADY AKADEMII NAUK SSSR* **104** 82–4
[28] von Batchelder F.W. and Raeuchle R.F. 1957 The structure of a new series of MBe_{12} compounds *Acta Crystallogr.* **10** 648–9
[29] Zalkin A., Sands D.E., Bedford R.G. and Krikorian O.H. 1961 The beryllides of Ti, V, Cr, Zr, Nb, Mo, Hf and Ta *Acta Crystallogr.* **14** 63–5
[30] Collins D.M. and Mahar M.C. 1984 The redetermination of the structure of beryllium–molybdenum $MoBe_{12}$ *Acta Crystallogr.* C **40** 914–5
[31] Cherkashin E.E., Gladyshevskii E.I., Kripyakevich P.I. and Kuz'ma Yu.B. 1958 X-ray structural analysis of certain systems of transition metals *Russian J. Inorg. Chem.* **3** 135–41
[32] Murphy S.T. 2014 Tritium solubility in Li_2TiO_3 from first-principles simulations *J. Phys. Chem.* C **118** 29525–32
[33] Vérité G., Domain C., Fu C.-C., Gasca P., Legris A. and Willaime F. 2013 Self-interstitial defects in hexagonal close packed metals revisited: evidence for low-symmetry configurations in Ti, Zr, and Hf *Phys. Rev.* B **87** 134108
[34] Burr P.A., Wenman M.R., Gault B., Moody M.P., Ivermark M., Rushton M.J.D., Preuss M., Edwards L. and Grimes R.W. 2015 From solid solution to cluster formation of Fe and Cr in α-Zr *J. Nucl. Mater.* **467** 320–31
[35] Kröger F. and Vink H. 1956 Relations between the concentrations of imperfections in crystalline solids *Solid state Phys.* **3** 307–435
[36] Predel B. 1992 Be–Ti (Beryllium–Titanium) *B-Ba – C-Zr* ed O. Madelung (Berlin: Springer) pp 1–2
[37] Predel B. 1992 Be–Mo (Beryllium–Molybdenum) *B-Ba – C-Zr* ed O. Madelung (Berlin: Springer) pp 1–3
[38] Predel B. 1992 Be–W (Beryllium–Tungsten) *B–Ba – C-Zr* ed O. Madelung (Berlin: Springer) pp 1–2
[39] Okamoto H. 2012 Be–V (Beryllium–Vanadium) *J. Phase Equilib. Diffus.* **33** 341
[40] Paine R.M., Carrabine J.A. and IUCr 1960 Some new intermetallic compounds of beryllium *Acta Crystallogr.* **13** 680–1